Computational Study of the Flow of Newtonian Fluid Through A Straight Channel and Lid-Driven Cavity

Jinan Raad Abdul-Jabbar*, Alaa H. Al-Muslimawi, Ihssan A. Fadhel
Department of Mathematics, College of Science, University of Basrah, Basrah, Iraq

Abstract

This article aims to introduce a numerical study of two different incompressible Newtonian fluid flows. The first type of flow is through the straight channel, while the second flow is enclosed within a square cavity and the fluid is moved by the upper plate at a specific velocity. Numerically, a Taylor-Galerkin\ pressure-correction finite element method (TGPCFEM) is chosen to address the relevant governing equations. The Naiver-Stoke partial differential equations are usually used to describe the activity of fluids. These equations consist of the continuity equation (conservation of mass) and the time-dependent conservation of momentum, which are preserved in Cartesian coordinates. In this study, the effect of Reynolds number (Re) variation is presented for both problems. Here, the influence of Re on the convergence rate and solution behavior is provided. Findings display that, there is a significant impact of Re upon the temporal convergence rates of velocity and pressure. As well, the rate of convergence increases as the values of Re are risen. For the cavity problem, one can infer that, as the Reynolds number rises, the size of the vortex is reduced.

Keywords: Finite element methods, Naiver-Stoke equations, Newtonian fluid, Galerkin method, Lid driven cavity.

دراسة حسابية لتدفق السائل النيوتوني عبر القناة المستقيمة والتجويف الذي يحركه الغطاء

جنان رعد عبد الجبار*, علاء حسن المسلماوي , احسان عقيل فاضل

قسم الرياضيات , كلية العلوم , جامعة البصرة , البصرة , العراق

الخلاصة

تهدف هذه المقالة إلى تقديم دراسة عددية لاثنين من تدفقات السوائل النيوتونية المختلفة غير القابلة للضغط. النوع الأول من التدفق عبر قناة مستقيمة، بينما النوع الثاني يتم إحاطة التدفق داخل تجويف مربع ويتم تحريك السائل بواسطة اللوحة العلوية بسرعة محددة. عدديًا، تم اختيار طريقة العناصر المحدودة لتصحيح الضغط تايلور-جاليركين (TGPCFEM) لمعالجة المعادلات الحاكمة ذات الصلة. عادةً ما تُستخدم المعادلات التفاضلية الجزئية Naiver–Stoke لوصف نشاط السوائل. تتكون هذه المعادلات من معادلة الاستمرارية (حفظ الكتلة) وحفظ الزخم المعتمد على الوقت، والتي يتم حفظها في الإحداثيات الديكارتية. في هذه الدراسة، تم عرض تأثير تباين عدد رينولدز لكلتا المشكلتين. هنا، يتم توفير تأثير Re على معدل التقارب وسلوك الحل. تظهر النتائج أن هناك تأثيرًا كبيرًا لـ Re على معدلات التقارب الزمني للسرعة والضغط. كذلك، يزداد

_____
*Email: genan.s712@gmail.com

معدل التقارب كلما ارتفعت قيم Re. بالنسبة لمشكلة التجويف، يمكن للمرء أن يستنتج أنه كلما ارتفع رقم رينولدز ،

قل حجم الدوامة.

1.Introduction

The numerical analysis of differential equations that govern the incompressible Newtonian fluid flow through straight channel and lid-driven cavity has received some great interest in the field of fluid dynamics. These types of fluid are usually governed by two differential equations; called conservation of mass and time-dependent conservation of momentum, which are offered here in cartesian coordinates under isothermal conditions (see Bird et al. 1987 for details). Geometrically, these problems appear at first sight to be simple, but it has a very important role in the field of fluid research in various industries. In the first problem, Poiseuille (*Ps*) flow along a two-dimensional planar straight channel, under isothermal condition is provided. In contrast, the lid square driven cavity problem is presented in this study as well. This flow is an idealized representation of several engineering situations, such as the flow over cutouts and repeated slots on the walls of heat exchangers or on the surface of aircraft bodies. In addition, as it is well known there are several structures of the lid-driven cavity depending upon boundary conditions, for example, single wall driven, parallel wall driven and anti-parallel wall driven etc. [1]. Here, we concern with the single upper wall driven, where the fluid is motioned by the upper-plate (lid) at a specific velocity. This problem has been investigated quite extensively as a numerical normative problem and as a test base for studying specific physical impacts, see [2]. Several numerical studies have been conducted and extended to steady incompressible flow in a driven cavity and are covered in the literature [3-8].

Numerically, a semi-implied Taylor-Galerkin/pressure-correcting finite element method (TG/PC-FEM) is applied in the temporal gradient. This approach is introduced by Townsend and Webster [9] to address incompressible flows of Newtonian and non-Newtonian fluids. In this method, the variables of velocity and pressure are decomposed (known primitive variable formulations), and this idea was inspired by Corinne's investigation [10]. Under this scheme, two main directions were taken to treat the governing equations. The first direction includes the fractal step method, which is favored by Gresho et. al. [11] and Donea et. al.[12]. Also, based on the velocity correction approach another direction is taken to solve the governing flow equations (see Kawahara and Ohmiya [14]). In addition, this approach includes two phases, the first being the Taylor- Galerkin method, which is a two-step Lax Wendroff time-step action (prediction corrector), extractor via Taylor series expansion in time (Donea [16], Zinenkiewicz et al. [17]). The second phase is the pressure correction method accommodate the incompressibility constraint to assure second-order thoroughness in time (see Hawken et al. [18], Aboubacar et al. [19]). The scheme is applied to triangular FE meshes, with pressure nodes located at the vertices and velocity components at both the vertical points and the middle nodes. Amazing attention was spent to treat the flow problems in the cartesian coordinates by using *TS-TG/PC-M* , see for example [15], [18-20].

The main motivation of this present study is the treatment of flow problems in Cartesian coordinates using Taylor-Galerkin/ pressure correction approach. In this context, two benchmark problems are studied; Poiseuille flow along a planar channel and lid-driven cavity of a square domain. The main findings in both problems are focused on the temporal convergence rate of the system solution to be a steady state under the variation of the Reynolds number.

The mathematical modelling of the motion of the Newtonian flows is present in the next section. The numerical approach is given in section 3. The problem of the discretization, the boundary conditions and the related numerical results are presented in sections 4 and 5, respectively.

2. Mathematical Modelling

For incompressible Newtonian isothermal flow in state of absence of body forces, the governing equations, which consist of momentum and continuity equations, can be stated as:

$$\nabla \cdot \mathbf{u} = 0. \tag{1}$$

$$\rho \frac{\partial u}{\partial t} = \nabla \cdot (2\mu d) \text{-}\rho u. \nabla u \text{-} \nabla p, \tag{2}$$

where, u, p, ρ and d are the velocity, pressure, density and rate of deformation for general flows, which can be expressed as

$$d = \frac{1}{2}(\nabla u + \nabla u^T). \tag{3}$$

Further, to define these equations in non-dimensional form, we introduce the scales and non-dimensional variables for the length L (the exact half-channel width), the velocity (the exact average velocity), pressure and viscosity as follows:

$$x^* = \frac{x}{U}, \ u^* = \frac{u}{U}, \ \mu^* = \frac{\mu}{\mu_\circ}, \ p^* = \frac{p}{\mu_\circ U/L}.$$

In addition, $Re = \rho \frac{UI}{\mu_s}$ represents the number of the non-dimensional set of Reynolds numbers. Regardless of the asterisk for clarity, the corresponding system of equations is shown under isothermal conditions

$$\frac{\partial u}{\partial t} = \frac{1}{Re}[\nabla \cdot (2\beta d) - Reu. \nabla u - \nabla p]. \tag{4}$$

In the Cartesian components, these equations can be written as:

$$\frac{\partial u_x}{\partial x} + \frac{\partial u_y}{\partial y} + \frac{\partial u_z}{\partial z} = 0, \tag{5}$$

$$\frac{\partial u_x}{\partial t} + u_x \frac{\partial u_x}{\partial x} + u_y \frac{\partial u_x}{\partial y} + u_z \frac{\partial u_x}{\partial z} = -\frac{1}{\rho}\frac{\partial p}{\partial x} + \frac{\mu}{\rho}\left(\frac{\partial^2 u_x}{\partial x^2} + \frac{\partial^2 u_x}{\partial y^2} + \frac{\partial^2 u_x}{\partial z^2}\right), \tag{6}$$

$$\frac{\partial u_y}{\partial t} + u_x \frac{\partial u_y}{\partial x} + u_y \frac{\partial u_y}{\partial y} + u_z \frac{\partial u_y}{\partial z} = -\frac{1}{\rho}\frac{\partial p}{\partial y} + \frac{\mu}{\rho}\left(\frac{\partial^2 u_y}{\partial x^2} + \frac{\partial^2 u_y}{\partial y^2} + \frac{\partial^2 u_y}{\partial z^2}\right), \tag{7}$$

$$\frac{\partial u_z}{\partial t} + u_x \frac{\partial u_z}{\partial x} + u_y \frac{\partial u_z}{\partial y} + u_z \frac{\partial u_z}{\partial z} = -\frac{1}{\rho}\frac{\partial p}{\partial z} + \frac{\mu}{\rho}\left(\frac{\partial^2 u_z}{\partial x^2} + \frac{\partial^2 u_z}{\partial y^2} + \frac{\partial^2 u_z}{\partial z^2}\right). \tag{8}$$

Where u_x, u_y and u_z represent the velocity in x direction, y direction and z direction, respectively.

3. Numerical method

A time semi-implied Taylor-Galerkin/ pressure-correction numerical scheme was adopted in this study. This scheme is based on a partial-staged approach that is first defined in the time domain by Taylor series expansions and includes a two-step Lax-Wendroff approach to capture second-order precision in time. Subsequently, the specific modification of the actuator split technology which is called the pressure correction method is adopted. This technique was developed by (Van Kan, 1986) which provides a second degree of correctness and overall strength by means of linear energy analysis. Historically, these schemes were proposed by Hawken et al., in 1990 in explicit form and then recognized by Townsend and Webster in 1987 who created a scheme which is named Taylor-Galerkin/ Pressure-correction (TGPC).

This algorithm can be presented in three distinct fractional stages for each time step as follows:

$\boldsymbol{Stage\ 1a}:\quad \frac{2Re}{\Delta t}[u^{n+\frac{1}{2}} - u^n] = \qquad [s(u^n, d^n) - \nabla p]^n,$ (9a)

$\quad\boldsymbol{Stage\ 1b}:\quad \frac{2Re}{\Delta t}[u^* - u^n] = s(u^{n+\frac{1}{2}}, d^{n+\frac{1}{2}}) - \nabla p^n,$ (9b)

$\quad\boldsymbol{Stage\ 2}:\quad \nabla^2(p^{n+1} - p^n) = \frac{Re}{\theta\Delta t}\nabla.u^*,$ (9c)

$\quad\boldsymbol{Stage\ 3}:\quad u^{n+1} = u^* - \frac{\theta\Delta t}{Re}\nabla(p^{n+1} - p^n).$ (9d)

In summary, the algorithm consists of three stages over each time $[t_n, t_{n+1}]$. First, at stage 1a, velocity components at half-time step $(n + \frac{1}{2})$ can be computed by using the data collected at the n time level. Then, in stage 1b, the velocity component u* of the full-time step is calculated from the data at levels n and $(n + \frac{1}{2})$. In stage 2, the pressure difference equation is solved over the full-time step range. Finally, the velocity field is recovered at stage 3, to complete the time step cycle.

To complete the process of the work, we need to get the matrix for the above stages by applying the essential steps in the finite element method. In this context, after finding the weak formulation of the stages ((9a), (9b), (9c) and (9d)), we introduce approximations $u(x, t)$ and $p(x, t)$ to the velocity and pressure respectively over finite dimensional function spaces as follows:

$$u(x, t) = \sum_{j=1}^{J_u} u_j(t)\phi_j(x),$$
$$p(x, t) = \sum_{j=1}^{J_p} p_j(t)\psi_j(x).$$ (10)

Such that J_u and J_p are the number total of the nodes and the number of vertices of the triangles only, respectively. Here, $u_j(t)$ and $p_j(t)$ represents a vector of nodal values of velocity and pressure and $\phi_j(x), \psi_j(x)$ are their respective basis (shape or interpolation) functions. In this context, quadratic shape functions of the velocity components in Cartesian coordinates are used. These functions are given in the usual coordinates as:

$$\begin{bmatrix} \phi_1 \\ \phi_2 \\ \phi_3 \\ \phi_4 \\ \phi_5 \\ \phi_6 \end{bmatrix}_{6X1} = \begin{bmatrix} L_1^2 - L_1(L_2 + L_3) \\ L_2^2 - L_2(L_3 + L_1) \\ L_3^2 - L_3(L_1 + L_2) \\ 4L_1L_2 \\ 4L_2L_3 \\ 4L_3L_1 \end{bmatrix}_{6X1} = \begin{bmatrix} 1 & 0 & 0 & -1 & 0 & -1 \\ 0 & 1 & 0 & -1 & -1 & 0 \\ 0 & 0 & 1 & 0 & -1 & -1 \\ 0 & 0 & 0 & 4 & 0 & 0 \\ 0 & 0 & 0 & 0 & 4 & 0 \\ 0 & 0 & 0 & 0 & 0 & 4 \end{bmatrix}_{6X6} \begin{bmatrix} L_1^2 \\ L_2^2 \\ L_3^2 \\ L_1L_2 \\ L_2L_3 \\ L_3L_1 \end{bmatrix}_{6X1}$$ (11)

Obviously, the vector of interpolation functions can be expressed in the matrix form as

$$\phi = [G][H].$$ (12)

In contrast, for pressure, the following linear shape function is used:

$$\begin{bmatrix} \psi_1 \\ \psi_2 \\ \psi_3 \end{bmatrix}_{3X1} = \begin{bmatrix} L_1 \\ L_2 \\ L_3 \end{bmatrix}_{3X1}.$$ (13)

Here, the vector of the linear shape function is symbolized by [E].

The three shape function L₁, L₂ and L₃ of the Cartesian coordinates are defined as follows:

$$L_i = \frac{1}{2A_{area}} (a_i + b_i x + c_i y), \quad (\forall i = 1,2,3). \tag{14}$$

Where, A_{area} is the area of the triangle of the element and a_i, b_i and c_i are coefficients. Thus, the corresponding a TGPC form of equations ((9a), (9b), (9c) and (9d)) can be written in matrix form as , see [18]:

$$\textbf{\textit{Stage 1a}:} \quad [\frac{2Re}{\Delta t}M + \frac{1}{2}S](U^{n+\frac{1}{2}} - U^n)$$
$$= \{-[S + ReN(U)]U + L^T p\}^n, \tag{15a}$$

$$\textbf{\textit{Stage 1b}:} \quad [\frac{Re}{\Delta t}M + \frac{1}{2}S](U^* - U^n) = \{-SU + L^T p\}^n -$$
$$(Re[N(U)U])^{n+\frac{1}{2}}, \tag{15b}$$

$$\textbf{\textit{Stage 2}:} \quad K(P^{n+1} - p^n) =$$
$$-\frac{Re}{\theta\Delta t}LU^*, \tag{15c}$$

$$\textbf{\textit{Stage 3}:} \quad \frac{Re}{\Delta t}M(U^{n+1} - U^*) = \theta L^T(P^{n+1} -$$
$$p^n). \tag{15d}$$

Such that,

$$M^{xx} = M^{yy} = \int_{\Omega^e} \phi\phi^T \, d\Omega, \tag{16}$$

$$[C(u_x, u_y)] = \int_{\Omega^e} (\phi\phi^T u_x \frac{\partial\phi^T}{\partial x} + \phi\phi^T u_y \frac{\partial\phi^T}{\partial y}) \, d\Omega, \tag{17}$$

$$S^{xx} = \int_{\Omega^e} \left[2\frac{\partial\phi}{\partial x}\frac{\partial\phi^T}{\partial x} + \frac{\partial\phi}{\partial y}\frac{\partial\phi^T}{\partial y} \right] d\Omega, \tag{18}$$

$$S^{xy} = (S^{yx})^T = \int_{\Omega^e} \left[\frac{\partial\phi}{\partial y}\frac{\partial\phi^T}{\partial x} \right] d\Omega, \tag{19}$$

$$S^{yy} = \int_{\Omega^e} \left[\frac{\partial\phi}{\partial x}\frac{\partial\phi^T}{\partial x} + 2\frac{\partial\phi}{\partial y}\frac{\partial\phi^T}{\partial y} \right] d\Omega, \tag{20}$$

$$\ell_x = \int_{\Omega^e} \left[\psi\frac{\partial\phi^T}{\partial x} \right] d\Omega, \qquad \ell_y = \int_{\Omega^e} \left[\psi\frac{\partial\phi^T}{\partial y} \right] d\Omega, \tag{21}$$

$$K = \int_{\Omega^e} \left[\frac{\partial\psi}{\partial x}\frac{\partial\psi^T}{\partial x} + \frac{\partial\psi}{\partial y}\frac{\partial\psi^T}{\partial y} \right] d\Omega. \tag{22}$$
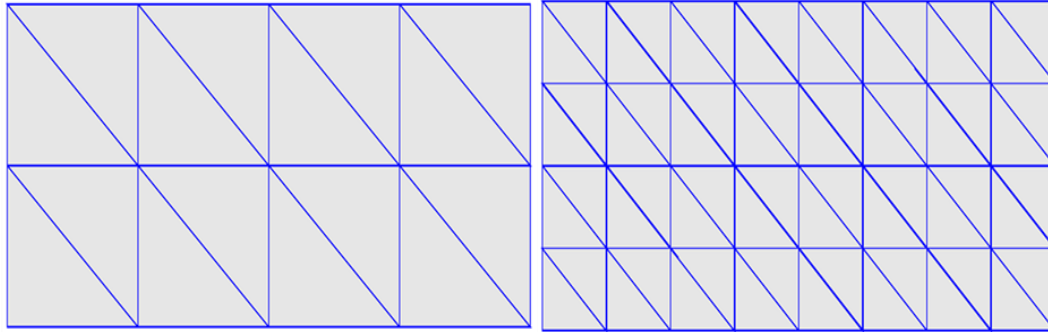
4. Test Problems and Boundary conditions

To confirm the algorithm, we review two problems, regarded as benchmarks in the Newtonian regime of interest. The first problem is the flow of Poiseuille through a straight channel with two axial dimensions under isothermal conditions. For this purpose, four triangular finite elements mesh are implemented: M1(4×4), M2(8×8), M3(14×12), M4(40×40) with the same length, as shown in Figure 1(a-d) (characteristics of a typical finite element mesh are included in Table 1). A second example concerns a driven cavity problem, where the fluid is driven by the upper plate (lid) at a given velocity as illustrated in Figure 1e. Here, triangular finite elements mesh is used as well; M5(10×10).
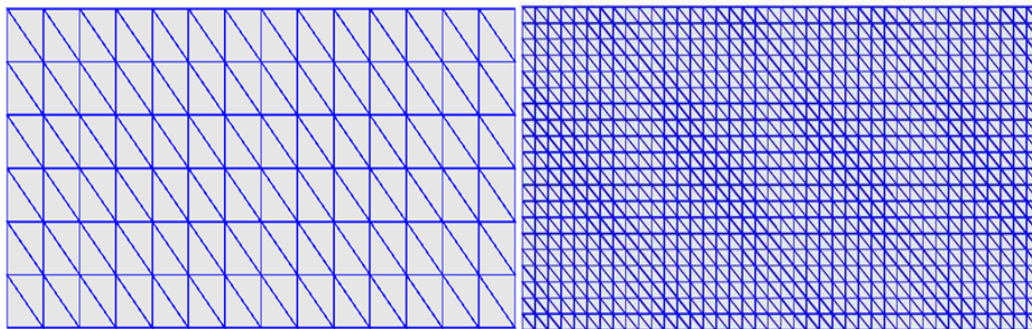
Table 1: Parameters that impact the mesh

Mesh	Total elements	Total nodes	Pressure nodes
M1	16	45	15
M2	64	153	45

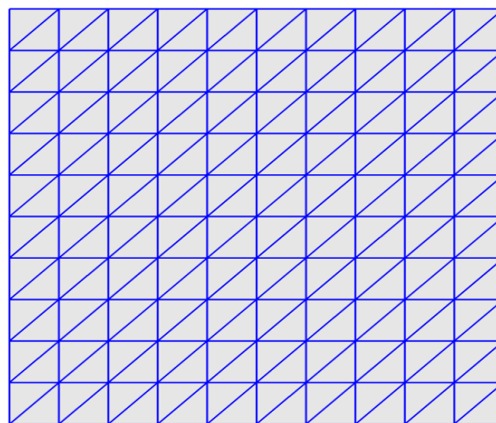|			
M3	168	377	105
M4	1600	2460	861
M5			

(a) M1 (4 × 4) mesh   **(b) M2 (8 × 8) mesh**

(c) M3 (14 × 12) mesh   **(d) M4 (40 × 40) mesh**

(f)   M5 (10 × 10) mesh

Figure 1 : mesh patterm

Boundary conditions (BCs): The setting of BCs for the two test problems is put as follows:

(a) Channel problem:
(1) Poiseuille flow(Ps) at the entrance is specified with zero radial velocity.
(2) Non-slip BCs is applied to the upper and lower walls of the channels.
(3) Zero radial velocity is applied and zero pressure is applied to the outlet of the channels.
 (b) Driven cavity problem:
(1) At the upper boundary, the tangential velocity with a variable profile of type $U = 16x^2(1 - x)^2$ is applied to pay the fluid flow in the cavity with a variable profile of type.
(2) No-slip BCs is applied on the remaining three walls.
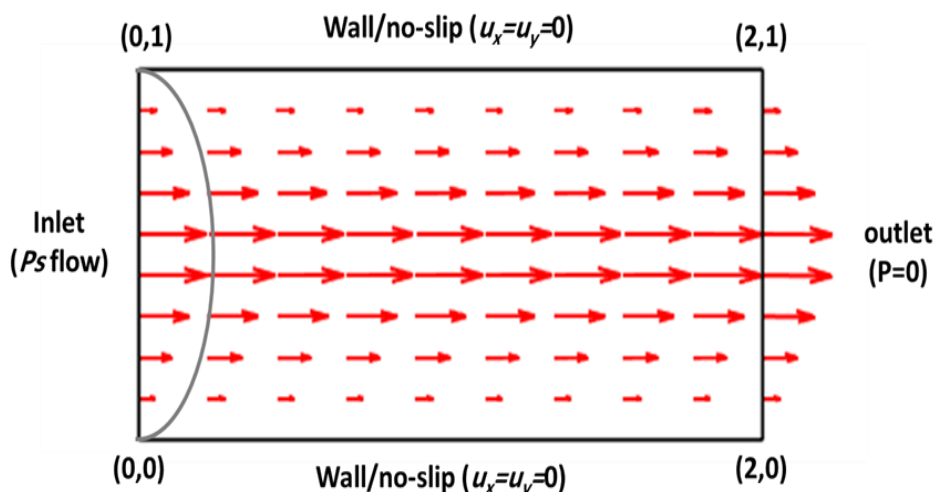
Figure 2: Schema for flow problem, boundary conditions

5. Numerical results

In the present study, two numerical examples are considered to calibrate the algorithm; a two-dimensional axisymmetric straight channel and driven cavity. Here, the numerical results of Newtonian flow are concerned on the effect of the Reynolds number (Re) on the solution components. The essential findings focus on the rate of convergence of velocity and pressure solutions under variation of Reynolds number. For that purpose, a time fractional-staged Taylor Galerkin/ pressure correction (TGPC) framework is applied. The convergence criteria are taken here as 10^{-6} and the typical Δt is $O(10^{-2})$. Al the results are introduced for the Cartesian coordinates system.

5.1 Straight channel

In Figure 3, velocity and pressure fields for fine mesh are presented at *Re*=1. As expected, the maximum axial velocity level is displayed along the center line of the channel with maxima of around (u=1.01791), and then gradually decreases. Also, the maximum level of the pressure (p=9.4244 units) has appeared at the inlet of the pipe decreases as we approach the outlet of the pipe. In addition, more details of the results for each mesh are in Table 2.
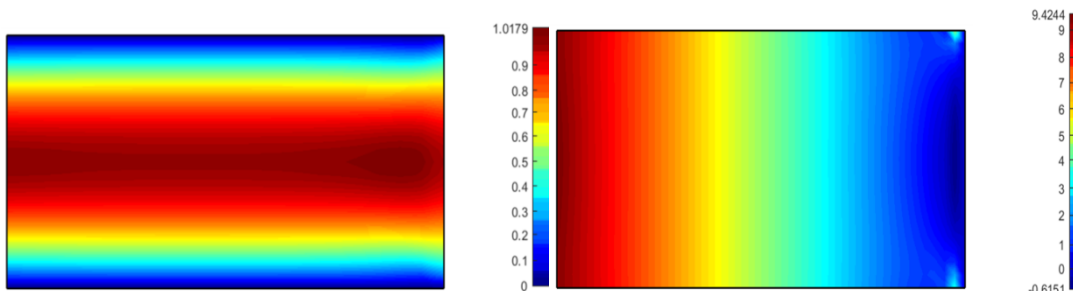
(a)   **(b)**
Figure 3: (a) Velocity field, (b) Pressure field: $Re = 1$

Table 2: The values of Maximum Velocity, Maximum Pressure with Meshes

Mesh	Max-Velocity	Max-Pressure
M1	1.0378	9.41895
M2	1.02224	9.40355
M3	1.02405	9.40496
M4	1.01791	9.4244

Pressure drop is plotted in Figure (4) for four different meshes and three different Reynolds number $Re=\{1,5,10\}$. The results reveal that, a linear pressure drop occurs throughout the center of the channel, after which the pressure reaches zero at the channel port. Additionally, in the case of Re-variation, the level of pressure rises with increasing Re, which reaches the highest level of 24 units with $Re=10$. Also, for the level of pressure, one can see that there is no change in the pressure when we refine the mesh.
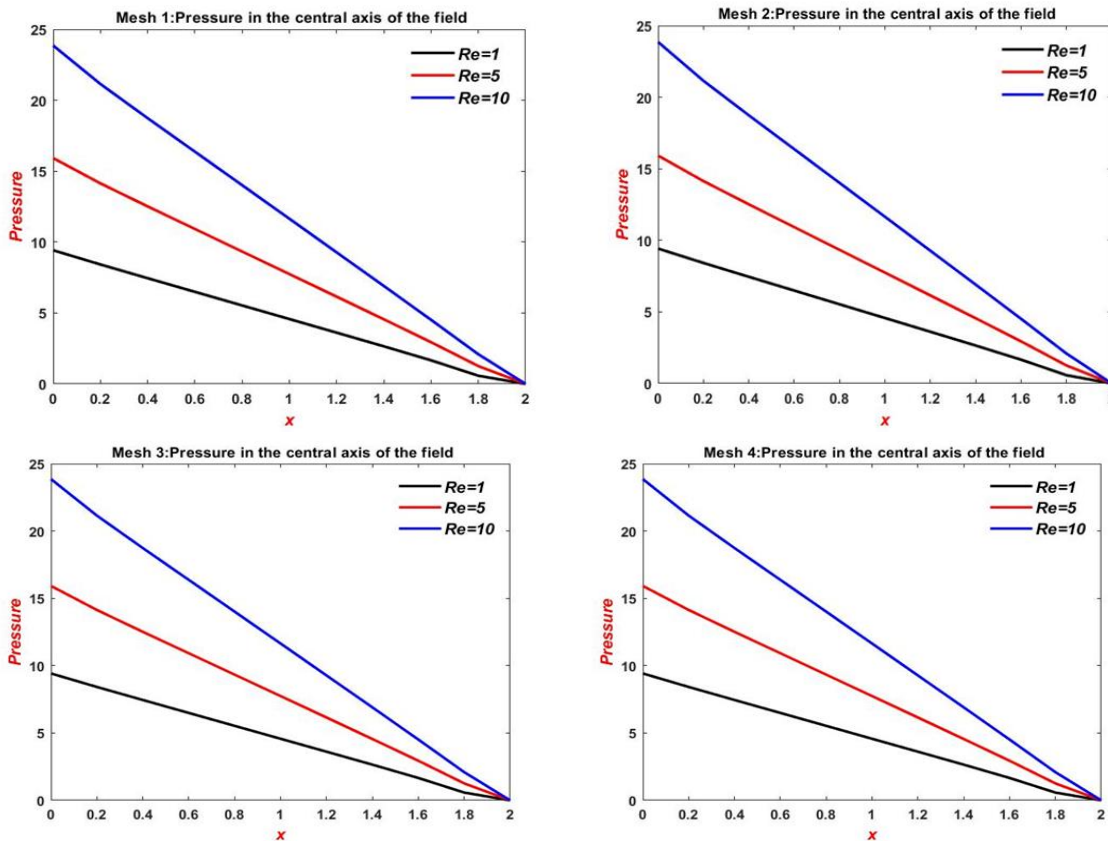

Figure 4: Pressure in the central axis of the field

The velocity gradients will be developed by increasing the Reynolds number, which gives the difficulties of convergence for the large Re numbers. Therefore, we devoted our attention to studying the impact of this factor on the level of velocity convergence. Figure (5) shows the rate of convergence of the axial velocity through the variation in the Reynolds number (Re) for four different meshes. The result reflects the effect of Re-variation on the axial velocity convergence, where the convergence rate increases corresponding to the increase in Re-level. Again, for the different meshes the level of convergence increases with the increase in mesh accuracy by a small amount.
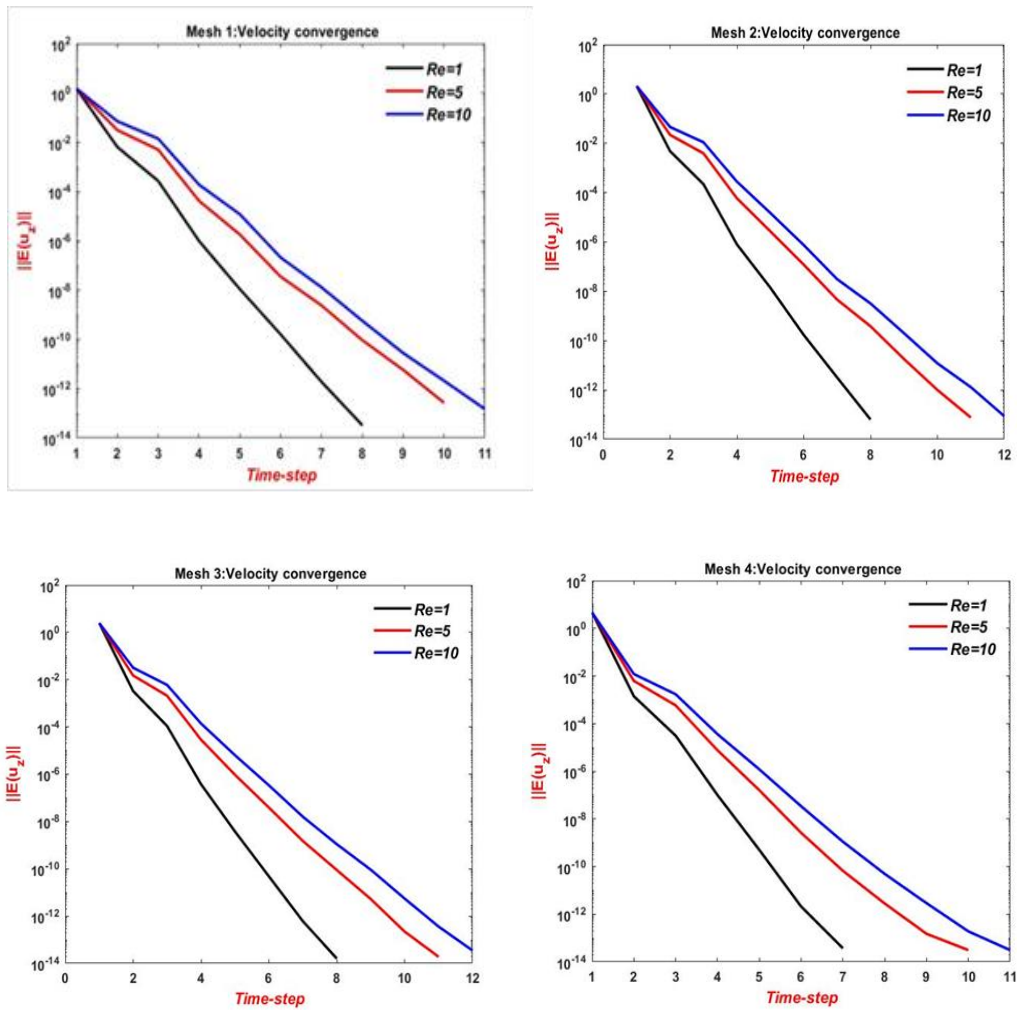
Figure 5: Convergence of axial velocity; *Re*-various

The convergent pressure is provided in Figure (6) for four different meshes through the variation in Reynolds number (*Re*). Here, the same feature of the convergent velocity is observed in the pressure case, where the level of convergence is increased with increasing *Re*-level. Here, for the difference meshes no obvious change in the level of convergence appeared.
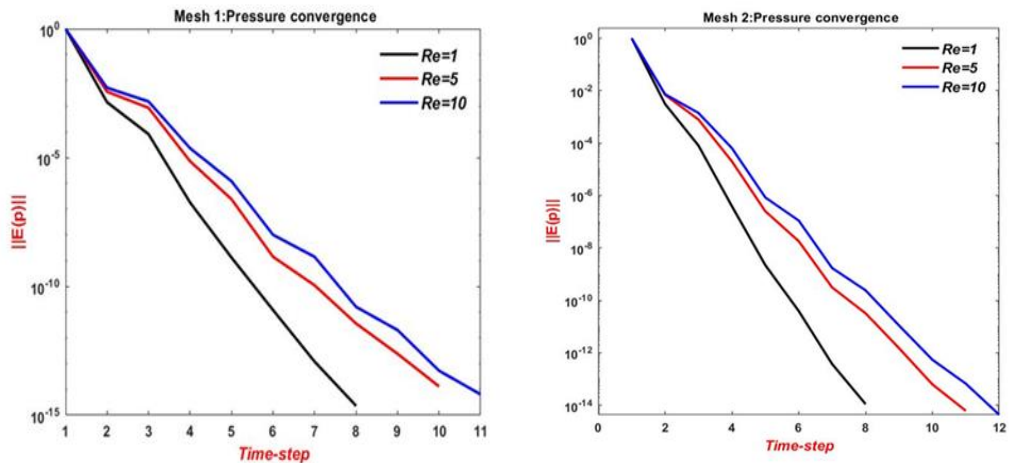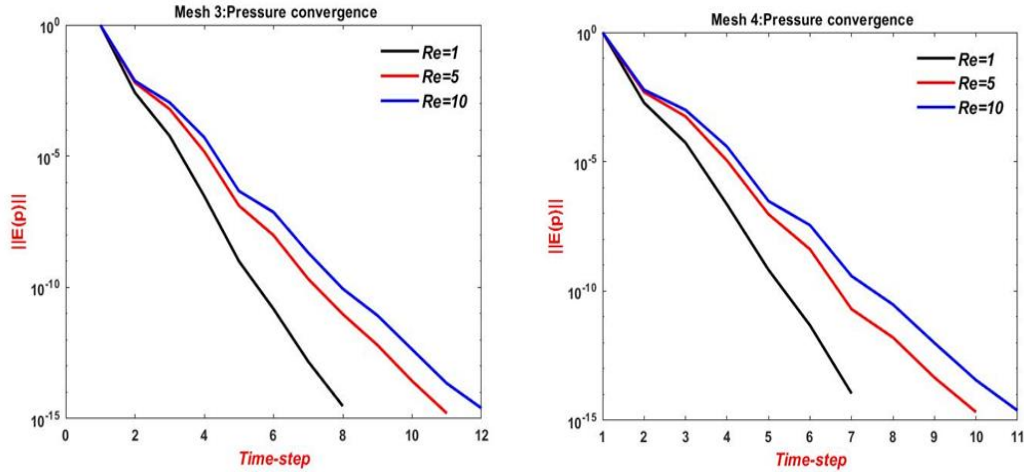
Figure 6: Convergence of pressure; *Re*-various

5.2 Driven cavity

Generally, this example is used as a standard test for evaluating numerical methods for incompressible flow (see Ghia et al., 1982, Hawken et al., 1990). In this problem, the flow is enclosed within a square cavity and the fluid is moved by the upper plate at a specific velocity. The velocity distribution in the axial direction is shown in Figure 7(a) at fixed *Re*=1. For the field, one can observe that, while there is a large gradient near the lid and dead zones in the lower left and lower right corners. Moreover, the pressure field is illustrated in Figure 7(b), which provides the region of low pressure in the center of the main vortex and in the upper left corner, and the stagnation point of the compound *x* of velocity in the upper right corner which characterized a large accumulated pressure. Figure 7(c) shows that the velocity vector at the upper of the cavity approaches U=1, where by the moving wall of the fluid flow is paid. The fluid is then paid toward the wall on the right, flowing downward before moving to the top of the left side of the cavity. Thus, this movement creates a big vortex in the center of the cavity. For a Reynolds number *Re*=1, we can note that the velocities at the center of the cavity are lower due to energy dissipation.


(a)   (b)
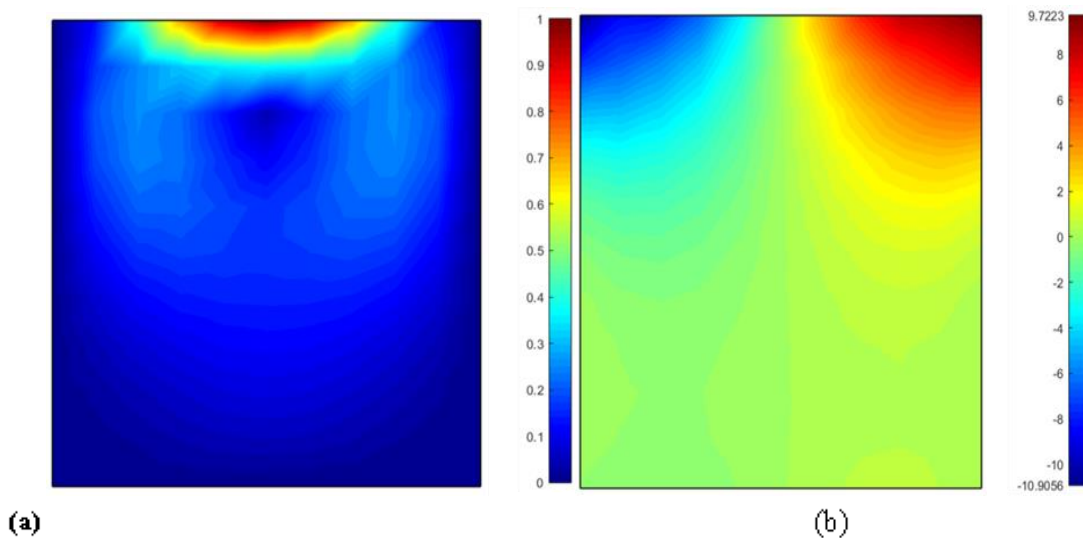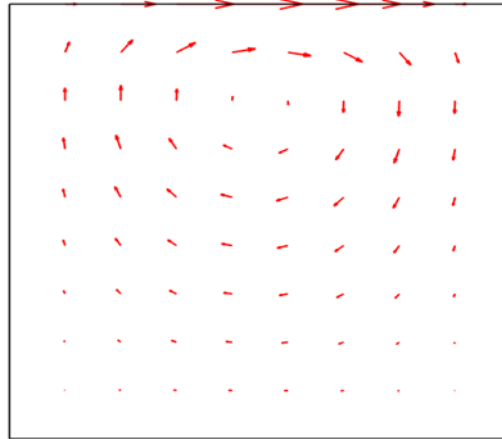
(c)

Figure 7: (a) Velocity field, (b) Pressure field, (c) velocity vector: *Re* = 1

Figure 8(a-f) shows streamline patterns of velocity flow through the variation in Reynolds number (*Re*). Here, we have been focused on the steady state vortex behavior as a function of rising Re. Generally, vortex size reduction is clearly apparent with increasing *Re*. In this context, for a Reynolds number less than 10, the vortex size at the cavity center is larger than that with Re≥10 due to the energy squander. Also, low Reynolds numbers, secedes the flow near the lower right and left corners and here two vortices formed. We can also see if the Reynolds number is raised, then there is more deadlock in flow, which causes her secession along the wall earlier and create bigger angle vortices. By increasing Reynolds number, vortices form in the down corners as well as one in the upper left corner.
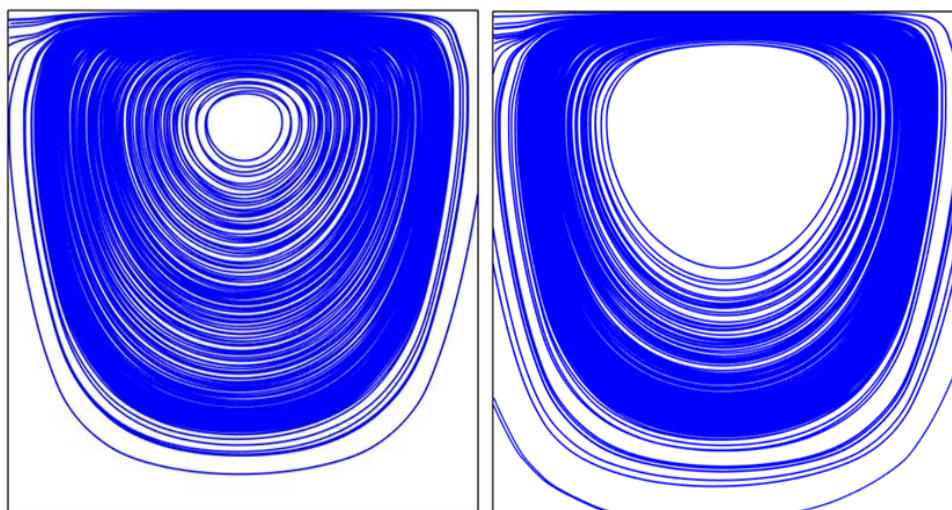
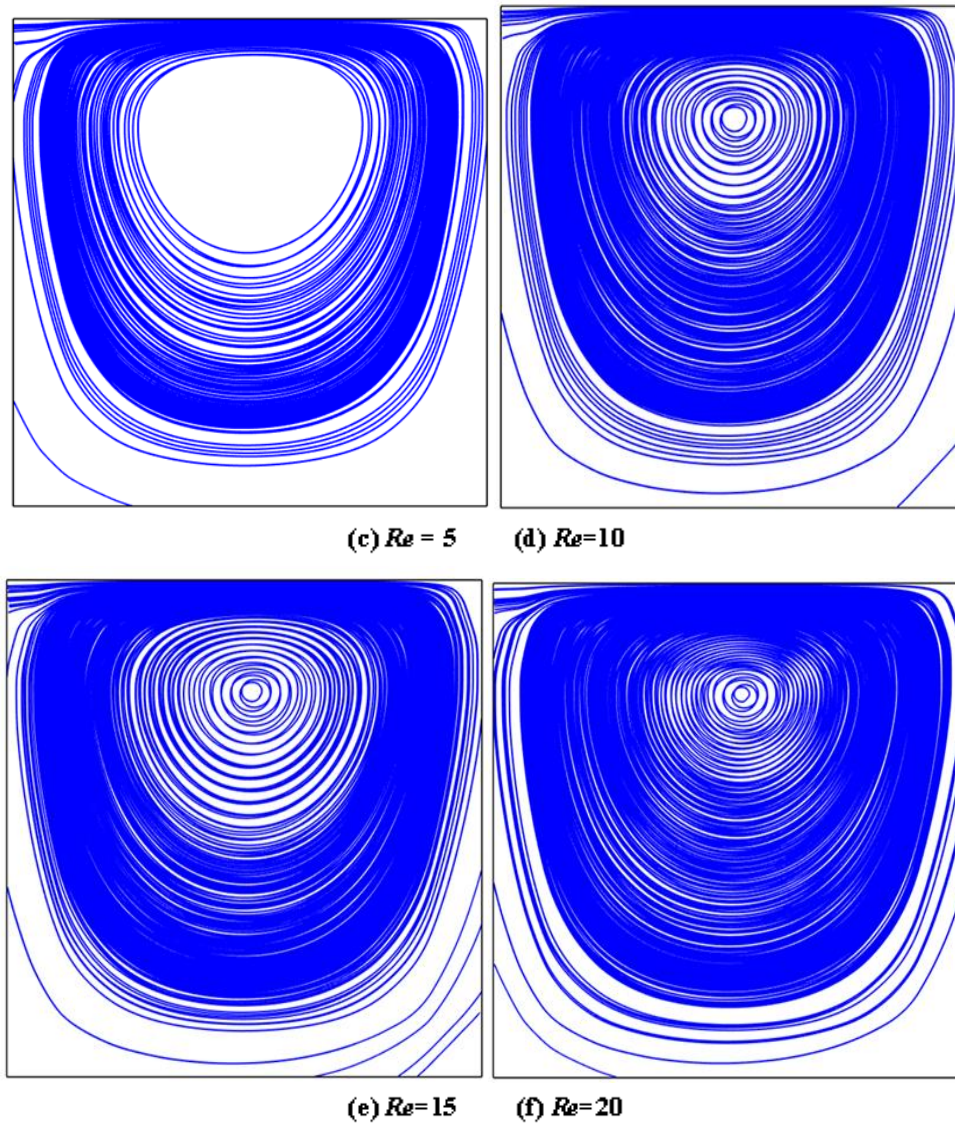**(a) Re=0.1**   **(b) Re = 1**

Figure 8: Streamline patterns for velocity flow; *Re*-variation

As stated above, the convergence rate of the axial velocity and pressure are shown in Figure (9) for different values of Reynolds number (*Re* = 1, 5, 10). In general, the level of velocity convergence at the same level of pressure convergence due to the effect of the nonlinear behavior. Additionally, and where expected, the results indicate that the rate of convergence increases with increasing Re values due to compression effects
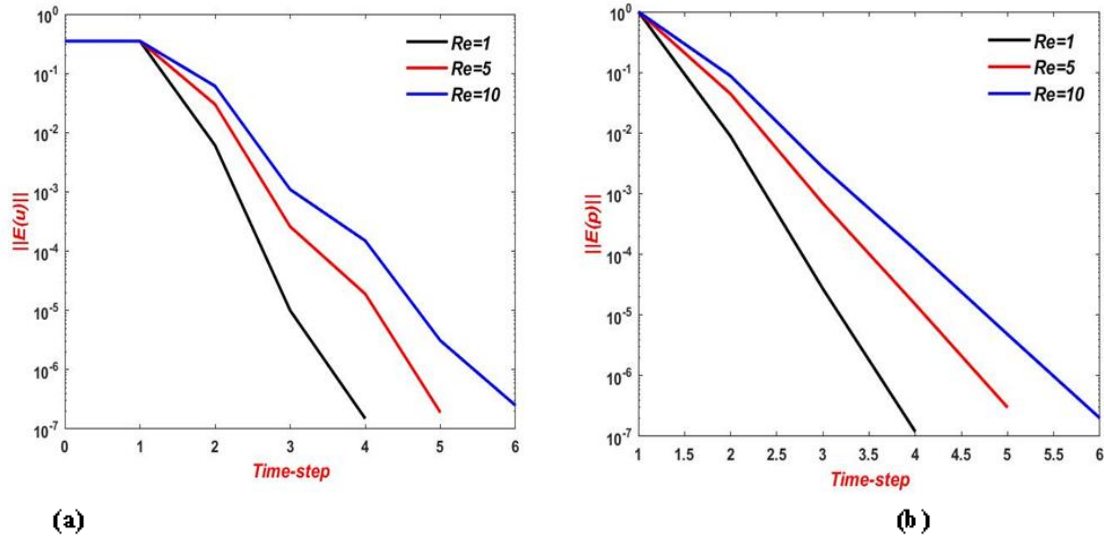
Figure 9: Convergence rate (a) velocity, (b) pressure; *Re*-variation

6. Conclusion

In this study, the numerical simulation for two different incompressible Newtonian fluid flows is achieved. The first type of flow is through the straight channel, while the second flow is enclosed within a square cavity and the fluid is moved by the upper plate at a specific velocity. To address the governing equations, the Taylor-Galerkin/ pressure-correction finite element method (TGPCFEM) is chosen. For that purpose, five finite element meshes are utilized. Convergence analysis is performed for the velocity and the pressure under the variation of Reynold's number for both problems. In this context, the results detect that there is a significant impact of *Re* upon the temporal convergence rates of velocity and pressure. Additionally, the rate of convergence is increasing as the values of *Re* are risen. As for the cavity problem, the results show that when the Reynolds number rises, the size of the vortex decreases and vortices form in the down corners as well as one in the upper left corner.

References
[1] O. Anthony, O. Iyiola, O. Miracle, "Numerical Simulation of the Lid Driven Cavity Flow with Inclined walls", *Journal of Scientific & Engineering Research*, vol. 4, no. 5, pp. 1681- 1694, 2013.
[2] F. Auteri, N. Parolini and L. Quartapelle, "Numerical Investigation on the Stability of Singular Driven Cavity Flow," *Journal of Computational Physics 183*, pp. 1-25, 2002.
[3] A. Amin, H. Samir, B. Oussama, "Numerical study of steady flow inside a lid-driven square cavity for Reynolds number up to 50000," *23ème Congrès Français de Mécanique*, pp. 1- 16, 2017.
[4] K. Venkatadri, S. Maheswari, C. V. Lakshmi and V. R. Prasad, "Numerical simulation of lid-driven cavity flow of micropolar fluid," *2nd International conference on Advances in Mechanical Engineering*, 2018,pp. 1-12.
[5] L. Shuguang, "Numerical simulation of non-Newtonian Carreau fluid in a lid-driven cavity," *Journal of Physics: Conference Series*, 2021, pp. 1-8.
[6] E. Erturk, "Discussions On Driven Cavity Flow," *International Journal for Numerical Methods in Fluids*, vol.60, pp. 275-294, 2009.
[7] J. Kushwah, K. C. Arora and M. Sharma, "CFD Simulation of Lid Driven Cavity Flow," *International Journal for Scientific Research & Development*, vol. 3, no. 10 , pp. 727- 729, 2015.

[8] S. Khorasanizade , J. M. M. Sousa, "A detailed study of lid-driven cavity flow at moderate Reynolds numbers using Incompressible SPH," *International Journal for Numerical Methods in Fluids*, vol.76, pp. 653–668, 2014.

[9] P. Townsend and M. F. Webster, *An algorithm for the three-dimensional transient simulation of non-Newtonian fluid flows*. In: Proc. Int. Conf. Num. Meth. Eng.: Theory and Applications, NUMETA, Nijhoff, Dordrecht, 1987.

[10] A. J. Chorin, *"*Numerical solution of the Navier-Stokes equations," *Math. Comput*, pp. 745-762, 1968.

[11] P. M. Gresho, R. L. Lee, and R. L. Sani, "On the time-dependent solution of the incompressible Navier-Stokes equations in two and three dimensions," *In Recent Advances in Numerical Methods in Fluids, Pineridge Press Limited, Swansea*, 1980.

[12] J. Donea, S. Giuliani, H. Laval, and L. Quartapelle, *"Finite element solution of the unsteady Navier-Stokes equations by a fractional step method*," *Comput. Methods Appl. Mech. Eng.,* vol. 30, pp. 53-73 , 1982.

[13] Yoo, J. Yul, and Yang Na. "A numerical study of the planar contraction flow of a viscoelastic fluid using the SIMPLER algorithm." *Journal of Non-Newtonian Fluid Mechanics 39*, no. 1, pp. 89-106, 1991.

[14] M. Kawahara and K. Ohmiya, "Finite element analysis of density flow using the velocity correction method," *Int. J. Num. Meth. Fluids*, vol. 5, pp. 981-993, 1985.

[15] A. H. Al-Muslimawi, "Taylor Galerkin Pressure Correction (TGPC) Finite Element Method for Incompressible Newtonian Cable-Coating Flows," *Journal of Kufa for Mathematics and Computer*, vol. 5,pp. 13-21, 2018.

[16] J. Donea, "A Taylor–Galerkin method for convective transport problems," *Int. J. Num. Meth. Eng.*, vol. 20, pp. 101–119, 1984.

[17] O. C. Zinenkiewicz, K. Morgan, J. Peraire, M. Vandati, R. Löhner, "Finite elements for compressible gas flow and similar systems," *In: 7th Int. Conf. Comput. Meth. Appl. Sci. Eng.*, 1985.

[18] D. M. Hawken, H. R. Tamaddon-Jahromi, P. Townsend, M. F. Webster, "A Taylor Galerkin based algorithm for viscous incompressible flow," *Int. J. Num. Meth. Fluids,* vol. 10, pp. 327- 351, 1990.

[19] D. M. Hawken, P. Townsend, and M. F. Webster, "Numerical simulation of viscous flows in channels with a step," *Comput. Fluids,* vol. 20, pp. 59-75, 1991.

[20] H. T. Jahromi, M. F. Webster, and P. R. Williams, "Excess pressure drop and drag calculations for strain-hardening fluids with mild shear-thinning: Contraction and falling sphere problems," *J. Non-Newton. Fluid Mech.,* pp. 939-950, 2011.

[21] B. K. Jassim, A. Al-Muslimawi, "Numerical analysis of Newtonian flows based on artificial compressibility AC method," J. of Al-Qadisiyah for *computer science and mathematics*, vol. 9, pp. 115-128, 2017.

[22] Sato, Toru, and Stephen M. Richardson. "Explicit numerical simulation of time-dependent viscoelastic flow problems by a finite element/ finite volume method." *Journal of Non-Newtonian Fluid Mechanics 51*, no. 3, pp. 249-275, 1994.

[23] A. H. Al-Muslimawi, S. D. Shakir, Numerical analysis of the Taylor Galerkin Pressure Correction (TGPC) finite element method for Newtonian fluid, *Journal of Basrah for Science*, Vol.5, No.8, 2015.

[24] Al-Muslimawi, Alaa H. "Numerical study for differential constitutive equations with polymer melts by using a hybrid finite-element/volume method." *Journal of Computational and Applied Mathematics*, vol. 308, pp. 488-498, 2016.

[25] R. Y. Yasir, A. H. Al-Muslimawi, "Numerical simulation of Power-Law inelastic fluid in channel by using finite element method," *Journal of Basrah for Science*, vol. 37, no.2, pp. 163-180, 2019.

[26] I. A. Fadhel, A. H. Al-Muslimawi, "Simulation of Newtonian axisymmetric pipe flow by using a Taylor Galerkin/pressure correction finite element method," *Journal of Basrah for Science*, vol. 38, no.2, pp. 198-222, 2020

[27] A. N. Abdulhasan, A. H. Al-Muslimawi, "Numerical investigation of extensional flow through axisymmetric conical geometries: Finite element method," *Journal of Basrah for Science*, vol. 38, no.3, pp. 399-421, 2020.